Construction of self-supporting bimetallic sulfide arrays as a highly efficient electrocatalyst for bifunctional electro-oxidation

Wenjun Liu[a,†], Liming Dai[b,†], Yiming Hu[a], Ku Jiang[a], Qian Li[a], Yilin Deng[a], Junjie Yuan[a], Jian Bao[a, *], Yucheng Lei[a, *]

a. School of Material Science & Engineering, Institute for Energy Research, Jiangsu University, Zhenjiang, Jiangsu, 212013, P. R. China.

b. School of Chemistry and Chemical Engineering , Nanjing University of Science and Technology, Nanjing, Jiangsu, 210094, P. R. China.

* Corresponding Authors should be addressed to: baojian@ujs.edu.cn, yclei@ujs.edu.cn.
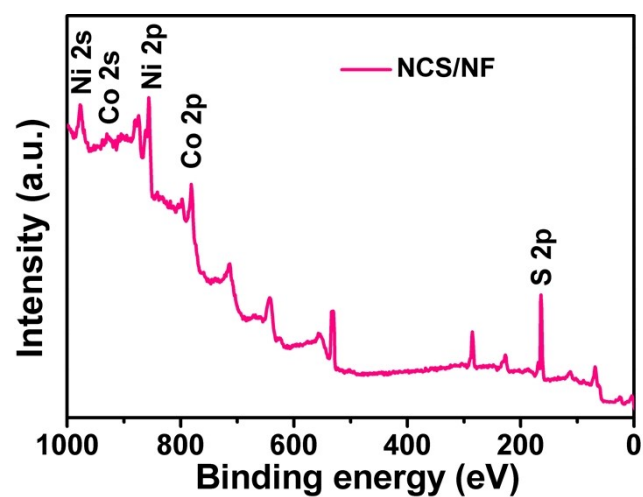
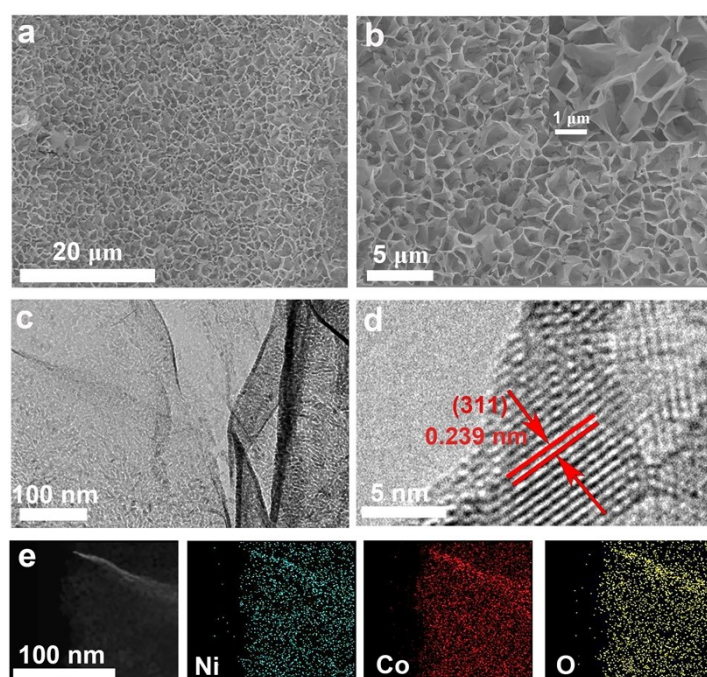**Figure S1.** XPS spectra for the NCS/NF sample.

Figure S2. (a) Low and (b) high magnification images of NCO/NF. (c) TEM image and (d) HR-TEM image of the NCO nanosheet. (e) EDX elemental mapping images of NCO sample.
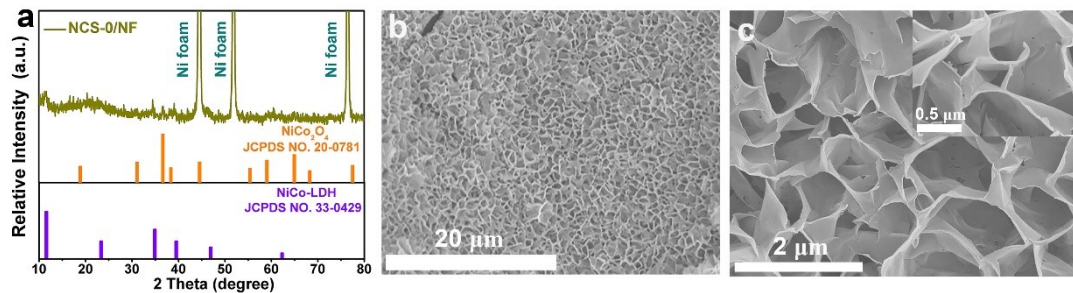
Figure S3. (a) XRD pattern of NCS-0/NF sample. (b) Low and (c) high magnification images of NCS-0/NF.
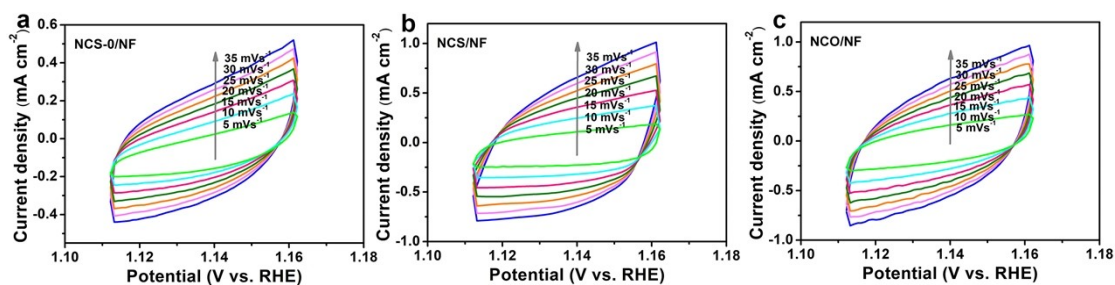

Figure S4. Double-layer capacitance measurements for determining electrochemically active surface area for (a) NCS-0/NF, (b) NCS/NF, and (c) NCO/NF.
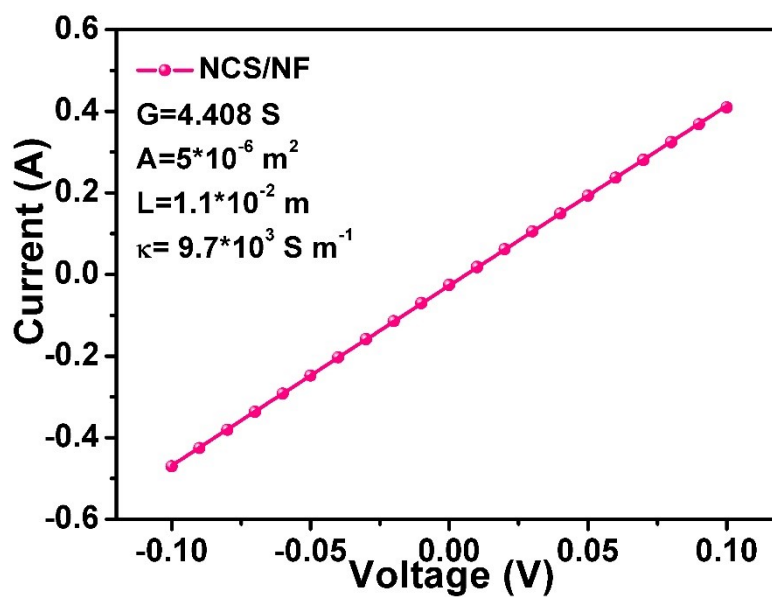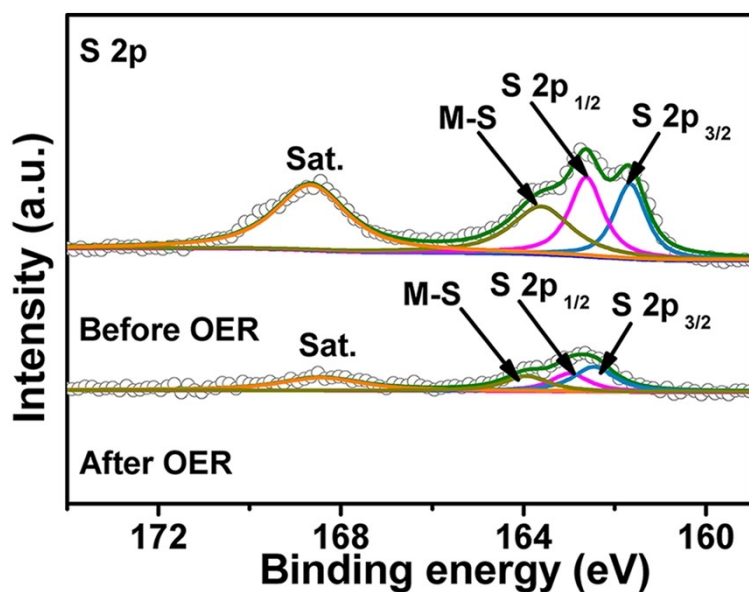

Figure S5. The I-U curves of NCS/NF.

Figure S6. S 2p spectra of the NCS/NF after the OER process.

Figure S7. (a) XRD pattern of NCO/NF sample before and after the OER processes.

(b) Co 2p, (c) Ni 2p, and (d) O 1s spectra of the NCO/NF before and after the OER

processes, respectively.

e S8. *In situ* Raman spectra of NCS/NF catalyst collected under multi-potential steps in 1.0 M KOH electrolyte for (a) OER, (b) OER in short range, and (c) HER.
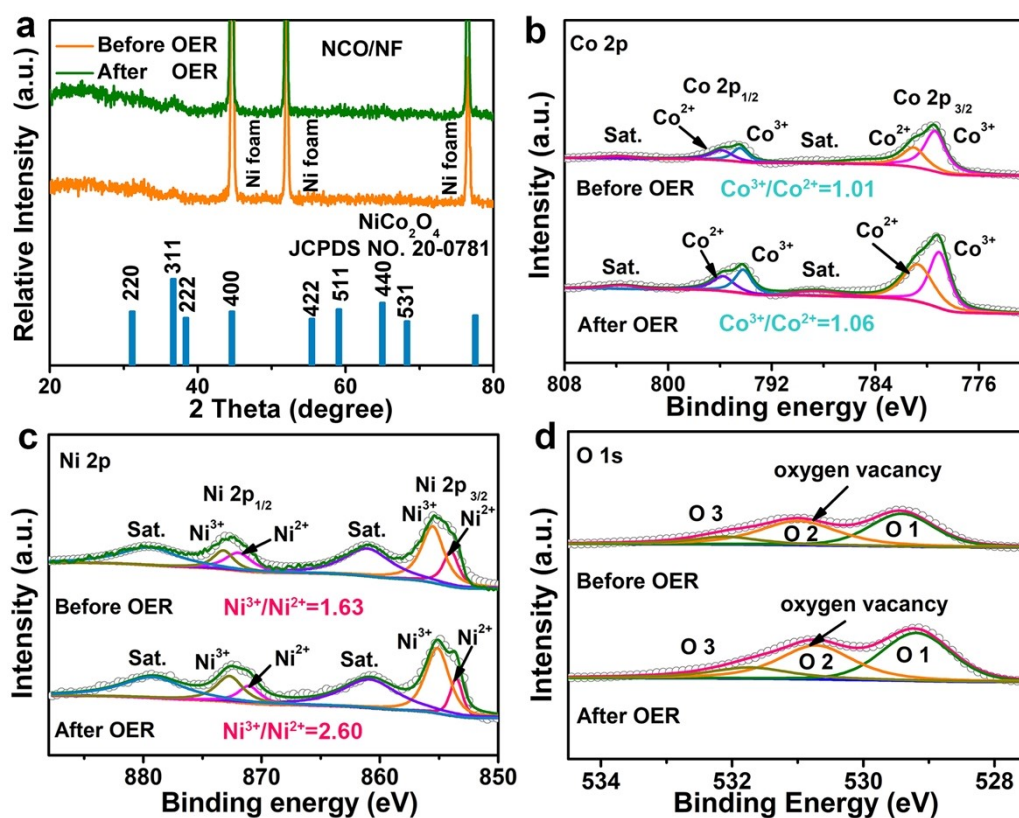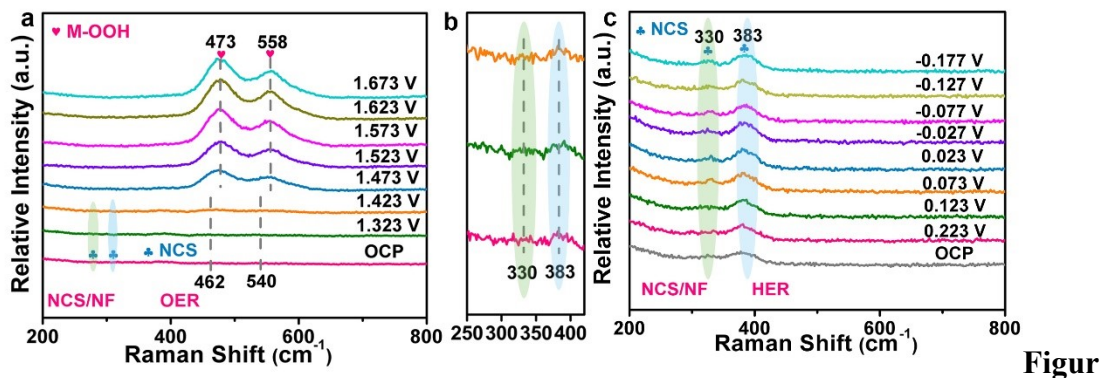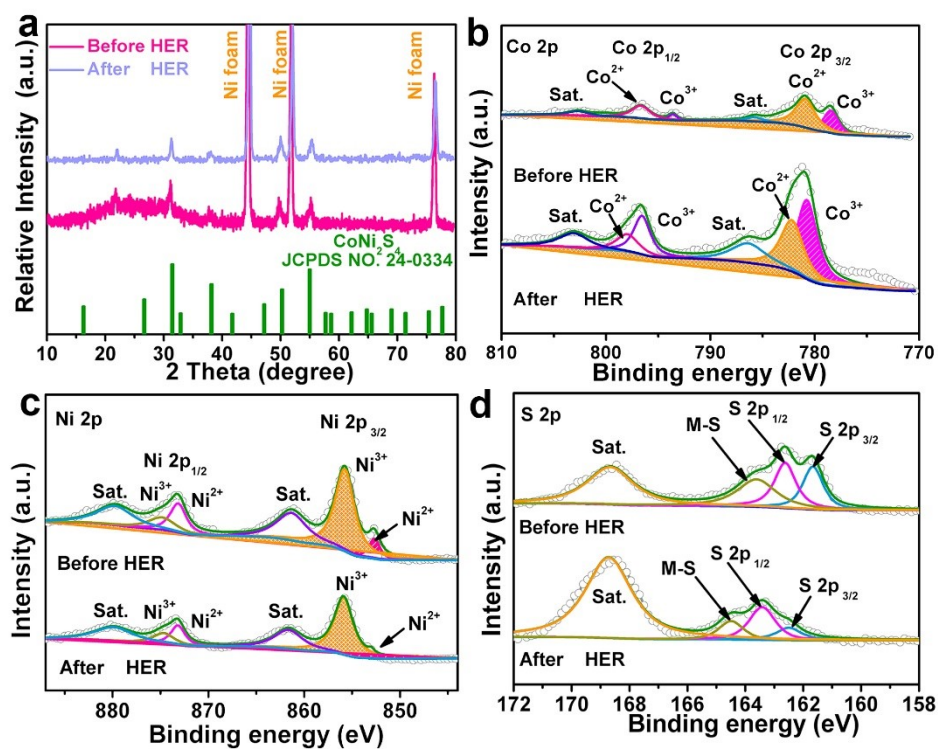

Figure S9. (a) XRD patterns of NCS/NF sample before and after the HER processes. (b) Co 2p, (c) Ni 2p, and (d) S 2p spectra of the NCS/NF before and after the HER processes, respectively.
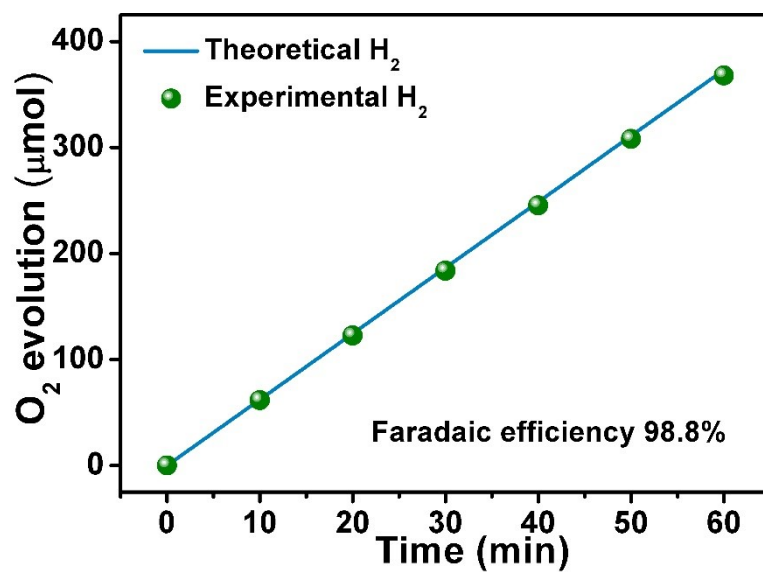
Figure S10 (a) Faradaic efficiency of NCS/NF at 20 mA·cm^{-2}.
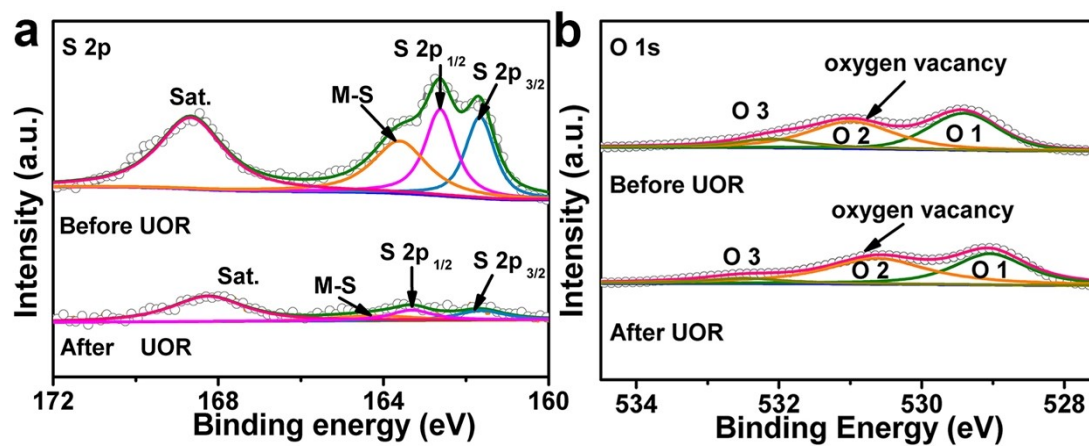
Figure S11. (a) S 2p spectra of the NCS/NF after the UOR process. (b) O 1s spectra of the NCO/NF after the UOR process.

Table S1 Comparison of the OER activity of several recently highly active catalysts.

Catalysts	Electrolyte	Overpotential /10 mA cm^{-2}	Reference
NCS/NF	1 M KOH	232 mV	This work
Fe-Ni$_3$S$_2$/FeNi foil	1 M KOH	282 mV	[S1]
Ni$_3$S$_2$/Ni foam	1 M KOH	260 mV	[S2]
NiCo$_2$S$_4$/Ni foam	1 M KOH	260 mV	[S3]
CNTs@Co-S/CP	1 M KOH	306 mV	[S4]
NiCoFeP	1 M KOH	273 mV	[S5]
NiCoFeB	1 M KOH	284 mV	[S6]
Ni$_3$Se$_4$ nanorod	1 M KOH	243 mV	[S7]
Fe-NiO nanoparticle	1 M KOH	297 mV	[S8]
Fe$_2$Ni$_2$N/Ni foam	1 M KOH	240 mV	[S9]
CoV$_2$O$_6$@V$_2$O$_5$/NRGO	1 M KOH	239 mV	[S10]
CoFe$_2$O$_4$@C/Ni foam	1 M KOH	240 mV	[S11]
NF/NiFe-LDH	1 M KOH	250 mV	[S12]
NF/Ni$_3$S$_2$	1 M KOH	260 mV	[S13]

Cu foil/Co$_3$O$_4$-C	1 M KOH	290 mV	[S14]
NiFe-NiCoO$_2$	1 M KOH	286 mV	[S15]
CuO@NiCo LDH/CF	1 M KOH	256 mV/20 mA cm^{-2}	[S16]
Co$_2$NiS$_{2.4}$(OH)$_{1.2}$	0.1 M KOH	279 mV	[S17]

Table S2 Impedance fitting results of NCS/NF and the compared samples in OER.

Sample	R_s/Ω	R_{ct}/Ω
NCS/NF	0.395	0.739
NCO/NF	0.287	1.409
NCS-0/NF	0.411	2.288

Table S3 Impedance fitting results of NCS/NF and the compared samples in HER.

Sample	R_s/Ω	R_{ct}/Ω
NCS/NF	0.485	0.311
NCO/NF	0.460	4.44
NCS-0/NF	0.349	45.11

Table S4 Comparison of the UOR activity of several recently highly active catalysts.

Catalysts	Electrolyte	Potential at 10 mA cm^{-2}	Reference
NCS/NF	1 M KOH + 0.33 M urea	1.31 V	This work
S-MnO$_2$	1 M KOH + 0.5 M urea	1.33 V	[S18]
NiSe$_2$	1 M KOH + 0.33 M urea	1.36 V	[S19]
NiO nanosheet array	1 M KOH + 0.33 M urea	1.38 V	[S20]
Ni(OH)$_2$ nanotube/NF	1 M KOH + 0.33 M urea	1.41 V	[S21]
Fe$_{11.1\%}$-Ni$_3$S$_2$/NF	1 M KOH + 0.33 M urea	1.44 V	[S22]
NiCo alloy	1 M KOH + 0.33 M urea	1.53 V	[S23]
Ni(OH)$_2$ nanocube array	1 M KOH + 0.33 M urea	1.55 V	[S24]
NiMo sheet array	1 M KOH + 0.33 M urea	1.37 V	[S25]
NiCo$_2$S$_4$ NS/Carbon cloth	1 M KOH + 0.33 M urea	1.317 V	[S26]
NiCo$_2$O$_4$	1 M KOH + 0.33 M urea	1.354 V	[S26]

NS/Carbon cloth			

Table S5 Impedance fitting results of NCS/NF and the compared samples in UOR.

Sample	R_s/Ω	R_{ct}/Ω
NCS/NF	0.346	0.302
NCO/NF	0.353	0.837

References:

[S1] C. Yuan, Z. Sun, Y. Jiang, Z. Yang, N. Jiang, Z. Zhao, U.Y. Qazi, W. Zhang, A. Xu, One-step in situ growth of iron-nickel sulfide nanosheets on FeNi alloy foils: high-performance and self-supported electrodes for water oxidation, Small 13 (2017) 1604161.

[S2] L. Feng, G. Yu, Y. Wu, G. Li, H. Li, Y. Sun, T. Asefa, W. Chen, X. Zou, High-index faceted Ni_3S_2 nanosheet arrays as highly active and ultrastable electrocatalysts for water splitting, J. Am. Chem. Soc. 137 (2015) 14023-14026.

[S3] A. Sivanantham, P. Ganesan, S. Shanmugam, Hierarchical $NiCo_2S_4$ nanowire arrays supported on Ni foam: an efficient and durable bifunctional electrocatalyst for oxygen and hydrogen evolution reactions, Adv. Funct. Mater. 26 (2016) 4661-4672.

[S4] J. Wang, H. Zhong, Z. Wang, F. Meng, X. Zhang, Integrated three-dimensional carbon paper/carbon tubes/cobalt-sulfide sheets as an efficient electrode for overall water splitting, ACS Nano 10 (2016) 2342-2348.

[S5] Y. Guo, J. Tang, Z. Wang, Y. Sugahara, Y. Yamauchi, Hollow porous heterometallic phosphide nanocubes for enhanced electrochemical water splitting, Small 14 (2018) 1802442.

[S6] Y. Li, B. Huang, Y. Sun, M. Luo, Y. Yang, Y. Qin, L. Wang, C. Li, F. Lv, W. Zhang, S. Guo, Multimetal borides nanochains as efficient electrocatalysts for overall water splitting, Small 15 (2019) 1804212.

[S7] J. Zhang, X. Tian, T. He, S. Zaman, M. Miao, Y. Yan, K. Qi, Z. Dong, H. Liu, B.Y. Xia, In situ formation of Ni_3Se_4 nanorod arrays as versatile electrocatalysts for electrochemical oxidation reactions in hybrid water electrolysis, J. Mater. Chem. A 6 (2018) 15653-15658.

[S8] K. Fominykh, P. Chernev, I. Zaharieva, J. Sicklinger, G. Stefanic, M. Döblinger, A. Müller, A. Pokharel, S. Böcklein, C. Scheu, T. Bein, D. Fattakhova-Rohlfing, Iron-doped nickel oxide nanocrystals as highly efficient electrocatalysts for alkaline water splitting, ACS Nano 9 (2015) 5180-5188.

[S9] M. Jiang, Y. Li, Z. Lu, X. Sun, X. Duan, Binary nickel-iron nitride nanoarrays as bifunctional electrocatalysts for overall water splitting, Inorg. Chem. Front. 3 (2016) 630-634.

[S10] F. Shen, Y. Wang, Y. Tang, S. Li, Y. Wang, L. Dong, Y. Li, Y. Xu, Y. Lan, CoV_2O_6–V_2O_5 coupled with porous N-doped reduced graphene oxide composite as a highly efficient electrocatalyst for oxygen evolution, ACS Energy Lett. 2 (2017) 1327-1333.

[S11] X. Lu, L. Gu, J. Wang, J. Wu, P. Liao, G. Li, Bimetal-organic framework derived $CoFe_2O_4$/C porous hybrid nanorod arrays as high-performance electrocatalysts for oxygen evolution reaction, Adv. Mater. 29 (2017) 1604437.

[S12] J. Luo, J. Im, M.T. Mayer, M. Schreier, M.K. Nazeeruddin, N. Park, S.D. Tilley, H.J. Fan, M. Grätzel, Water photolysis at 12.3% efficiency via perovskite photovoltaics and Earth-abundant catalysts, Science 345 (2014) 1593.

[S13] L. Feng, G. Yu, Y. Wu, G. Li, H. Li, Y. Sun, T. Asefa, W. Chen, X. Zou, High-index faceted Ni_3S_2 nanosheet arrays as highly active and ultrastable electrocatalysts for water splitting, J. Am. Chem. Soc. 137 (2015) 14023-14026.

[S14] T.Y. Ma, S. Dai, M. Jaroniec, S.Z. Qiao, Metal-organic framework derived hybrid Co_3O_4-carbon porous nanowire arrays as reversible oxygen evolution electrodes, J. Am. Chem. Soc. 136 (2014) 13925-13931.

[S15] R. Shi , J. Wang , Z. Wang , T. Li , Y. Song, Unique $NiFe$-$NiCoO_2$ hollow polyhedron as bifunctional electrocatalysts for water splitting, J. Energy Chem. 33 (2019) 74.

[S16] Y. Cao, T. Wang, X. Li, L. Zhang, Y. Luo, F. Zhang, A.M. Asiri, J. Hu,* Q. Liu * and X. Sun, A hierarchical CuO@NiCo layered double hydroxide core-shell nanoarray as an efficient electrocatalyst for the oxygen evolution reaction, Inorg. Chem. Commun. 8 (2021) 3049.

[S17] B. Wang, C. Tang, H. Wang, X. Chen, R. Cao, Q. Zhang, Core-branch CoNi hydroxysulfides with versatilely regulated electronic and surface structures for superior oxygen evolution electrocatalysis, J. Energy Chem. 38 (2019) 8.

[S18] S. Chen, J. Duan, A. Vasileff, S.Z. Qiao, Size fractionation of two-dimensional sub-nanometer thin manganese dioxide crystals towards superior urea electrocatalytic conversion, Angew. Chem. Int. Ed. 55 (2016) 3804-3808.

[S19] P. Xiong, X. Ao, J. Chen, J. Li, L. Lv, Z. Li, M. Zondode, X. Xue, Y. Lan, C. Wang, Nickel diselenide nanoflakes give superior urea electrocatalytic conversion, Electrochim. Acta 297 (2019) 833-841.

[S20] M. Wu, G. Lin, R. Yang, Hydrothermal growth of vertically-aligned ordered mesoporous nickel oxide nanosheets on three-dimensional nickel framework for electrocatalytic oxidation of urea in alkaline medium, J. Power Sources 272 (2014) 711-718.

[S21] R. Ji, D. Chan, J. Jow, M. Wu, Formation of open-ended nickel hydroxide nanotubes on three-dimensional nickel framework for enhanced urea electrolysis, Electrochem. Commun. 29 (2013) 21-24.

[S22] W. Zhu, Z. Yue, W. Zhang, N. Hu, Z. Luo, M. Ren, Z. Xu, Z. Wei, Y. Suo, J. Wang, Wet-chemistry topotactic synthesis of bimetallic iron-nickel sulfide nanoarrays: an advanced and versatile catalyst for energy efficient overall water and urea electrolysis, J. Mater. Chem. A 6 (2018) 4346-4353.

[S23] W. Xu, H. Zhang, G. Li, Z. Wu, Nickel-cobalt bimetallic anode catalysts for direct urea fuel cell, Sci. Rep. 4 (2014) 5863.

[S24] M. Wu, R. Ji, Y. Zheng, Nickel hydroxide electrode with a monolayer of nanocup arrays as an effective electrocatalyst for enhanced electrolysis of urea, Electrochim. Acta 144 (2014) 194-199.

[S25] Y. Liang, Q. Liu, A.M. Asiri, X. Sun, Enhanced electrooxidation of urea using $NiMoO_4 \cdot xH_2O$ nanosheet arrays on Ni foam as anode, Electrochim. Acta. 153 (2015) 456-460.

[S26] W. Zhu, M. Ren, N. Hu, W. Zhang, Z. Luo, R. Wang, J. Wang, L. Huang, Y. Suo, J. Wang, Traditional $NiCo_2S_4$ phase with porous nanosheet array topology on carbon cloth: a flexible, versatile and fabulous electrocatalyst for overall water and urea electrolysis, ACS Sustain. Chem. Eng. 6 (2018) 5011-5020.